CCFE
CULHAM CENTRE FOR FUSION ENERGY

UK Atomic Energy Authority

UKAEA-CCFE-CP(19)20

S. S. Henderson, M. Bernert, S. Brezinsek, M. Carr, M. Cavedon, R. Dux, D. S. Gahle, J. Harrison, B. Lipschultz, B. Lomanowski, A. Meigs, M. O'Mullane, F. Reimold, M. L. Reinke, S. Wiesen, the EUROfusion MST1 team, the ASDEX Upgrade team, JET contributors

An assessment of nitrogen concentrations from spectroscopic measurements in the JET and ASDEX Upgrade divertor

An assessment of nitrogen concentrations from spectroscopic measurements in the JET and ASDEX Upgrade divertor

S. S. Henderson, M. Bernert, S. Brezinsek, M. Carr, M. Cavedon, R. Dux, D. S. Gahle, J. Harrison, B. Lipschultz, B. Lomanowski, A. Meigs, M. O'Mullane, F. Reimold, M. L. Reinke, S. Wiesen, the EUROfusion MST1 team, the ASDEX Upgrade team, JET contributors

This paper has been submitted to
23rd International Conference on Plasma Surface Interactions in Controlled Fusion Devices (PSI), Princeton, NJ, USA, 17-22 June 2018

An assessment of nitrogen concentrations from spectroscopic measurements in the JET and ASDEX Upgrade divertor

S. S. Henderson[a], M. Bernert[b], S. Brezinsek[c], M. Carr[a], M. Cavedon[b], R. Dux[b], D. S. Gahle[d,a], J. Harrison[a], A. Kallenbach[b], B. Lipschultz[e], B. Lomanowski[f], A. Meigs[a], M. O'Mullane[d], F. Reimold[g], M. L. Reinke[h], S. Wiesen[c], the EUROfusion MST1 team[1], ASDEX Upgrade team[2], and JET contributors[3]

[a]*CCFE, Culham Science Centre, Abingdon, OX14 3DB, UK*
[b]*Max-Plank-Institut für Plasmaphysik, D-85748 Garching, Germany*
[c]*Forschungszentrum Jülich GmbH, Institut für Energie-und Klimaforschung, 52425 Jülich, Germany*
[d]*University of Strathclyde, Dept. of Physics, Glasgow, G4 0NG, UK*
[e]*University of York, York Plasma Institute, York, YO10 5DD, UK*
[f]*Aalto University School of Science, Dept. of Applied Physics, P.O. Box 11100, Aalto, FI-00076, Finland*
[g]*Max-Plank-Institut für Plasmaphysik, 17489 Greifswald, Germany*
[h]*Oak Ridge National Laboratory, Oak Ridge, TN 37831, USA*

Abstract

The impurity concentration in the tokamak divertor plasma is a necessary input for predictive scaling of divertor detachment, however direct measurements from existing tokamaks in different divertor plasma conditions are limited. To address this, we have applied a recently developed spectroscopic N II line ratio technique for measuring the N concentration in the divertor to a range of H-mode and L-mode plasma from the ASDEX Upgrade and JET tokamaks, respectively. The results from both devices show that as the power crossing the separatrix, P_{sep}, is increased under otherwise similar core conditions (e.g. density), a higher N concentration is required to achieve the same detachment state. For example, the N concentrations at the start of detachment increase from $\approx$ 2% to $\approx$ 9% as P_{sep} is increased from $\approx$ 2.5 MW to $\approx$ 7 MW, suggesting an approximately linear dependence on P_{sep}. The N concentrations from spectroscopy and from the ratio of D and N gas valve fluxes agree within the experimental uncertainty only in scenarios where the vessel surfaces are fully-loaded with N. This analysis provides a basis for future studies examining the parameters which affect the N concentration required to reach detachment.

Email address: stuart.henderson@ukaea.uk (S. S. Henderson)

[1]See the author lists of H. Meyer *et al*. 2017 Nucl. Fusion 57 102014
[2]A. Kallenbach *et al*. 2017 Nucl. Fusion 57 102015
[3]X. Litaudon *et al*. 2017 Nucl. Fusion 57 102001

Keywords: impurity, nitrogen, divertor, concentration, spectroscopy, tokamak

1. Introduction

Substantial seeding of impurities, e.g. with N, to reduce the plasma power exhaust impacting on plasma facing components has been used for a long time in tokamak research [1, 2, 3, 4]. Currently, measurements of the seeded impurity concentration in the divertor are limited [5, 6] and the amount required to facilitate detachment is currently not well understood. Goldston *et al*. [7] have recently developed a scaling law to predict the impurity concentration required to attain detachment, in terms of scrape-off layer plasma parameters such as the upstream density, separatrix power and poloidal magnetic field. To validate this model, the experimental impurity concentration is required, which has previously been estimated on ASDEX Upgrade (AUG) from the ratio of the main ion and seeding gas valve flux rates [8]. However, the accuracy of these N concentration estimates depends strongly on the amount of vessel wall pumping and release of the impurity and fuel species [9, 10].

To assess and compare with the gas valve flux rate measurements, this paper exploits a recently developed spectroscopic N II line ratio technique for measuring the N concentration in the divertor [11]. Since this new measurement technique is compatible with the spectrometer settings routinely used to measure Stark broadening [12, 13], there are a range of pulses from AUG and JET with suitable viewing geometries and diagnostic setup. The main aim of this paper is to demonstrate the robustness of the measurement in a wide range of discharges, recover the expected trends with divertor temperature (i.e. higher concentration in lower divertor temperature plasma for similar separatrix power and density), and to provide a basis for future studies examining the parameter dependencies of the impurity concentration required to facilitate detachment.

The paper is structured as follows. Section 2 details the experiment setup and the range of conditions from AUG and JET plasma. Section 3 outlines the model for calculating the nitrogen concentration. The measurements of the divertor nitrogen concentrations from AUG and JET are analysed in section 4. Lastly, the conclusions are drawn in section 5.

2. Experiment setup

For AUG, a total of 26 N-seeded, H-mode pulses are analysed with N II radiance measurements averaged over steady-state time-windows of at least 200 ms, where ELM periods are removed. The database includes a range of power crossing the separatrix ($P_{sep} = 2 - 10$ MW) and divertor temperatures $T_{div} = 3 - 50$ eV, at various fuelling and

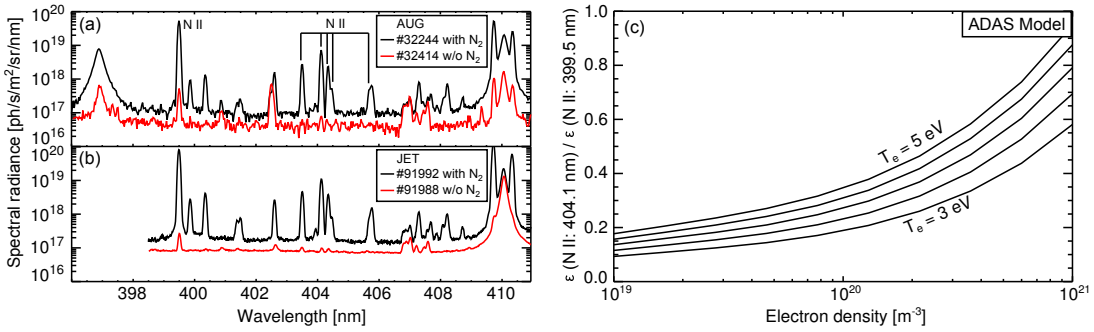

Figure 1: Time averaged spectrum measured in the (a) ASDEX Upgrade and (b) JET divertor with (black) and without (red) N_2 seeding. The ratio of two N II multiplet lines from a collisional-radiative model is shown for a range of electron temperatures and densities in (c).

N_2 seeding rates. Note that T_{div} is an AUG specific real-time estimate of the outer divertor temperature (assuming a very low inner divertor temperature) derived from shunt measurements of the thermo-electric current into the outer divertor [14]. This signal has been shown to agree well with the electron temperature near the strike point for attached conditions. The other plasma parameters relevant for scaling the impurity concentration required for detachment [7] (see section 4) are: the line-averaged interferometry measuring through the plasma edge to provide a proxy for the separatrix densities $n_{e,sep} = 3 - 5x10^{19}$ m^{-3}, which normalised to the Greenwald fraction correspond to $f_{GW,sep} = 0.22 - 0.42$; the poloidal magnetic field $B_p = 0.24 - 0.3$ T; and the plasma elongation $\kappa = 1.7 - 1.8$. A divertor Czerny Turner-like visible spectrometer [12] is used to measure the inter-ELM spectral radiance in the wavelength range 396 nm$< \lambda <$ 411 nm with an integration time of $\Delta t = 2.5$ ms.

On JET, a mirror-linked JET-ILW divertor spectrometer system [15] is used to measure the equivalent N II radiance with a temporal resolution of $\Delta t = 40$ ms. Due to the difficulties of obtaining inter-ELM measurements with the longer integration time, the analysis is limited to two low power, N_2-seeded L-mode discharges (#90419 and #90423, see [16] for further details). Both discharges are identical except for a change in N_2 seeding rate, with $P_{sep} = 2.5 - 2.7$ MW, $B_p \approx 0.4$, $f_{GW,sep} = 0.3 - 0.4$, and $\kappa \approx 1.65$. The equivalent real-time T_{div} measurement is not available on JET, and therefore the strike point temperature measured at the target by Langmuir probes, T_e^{tgt}, is used instead to characterise the detachment state.

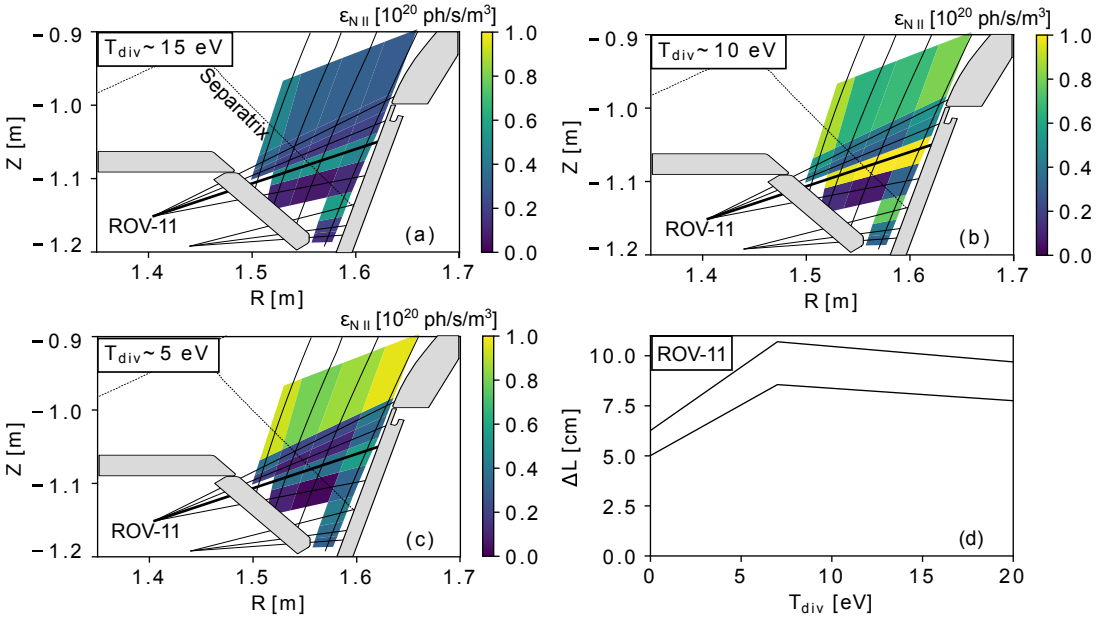

Figure 2: Inverted spectrometer sightline data showing the N II emission at 404.1 nm for three different divertor temperatures in AUG pulse #34971 in (a) - (c). The ROV-11 sightline used to analyse c_N is highlighted by the thick black line in each panel. The estimated ΔL profile is shown as a function of T_{div} in (d).

3. Concentration model

The N II radiance measurements from the divertor plasma are used to calculate the line-averaged nitrogen concentration, c_N, using

$$c_N = \frac{4\pi \int \epsilon_{NII} \Delta L}{(f_{N^+} PEC^{exc} + f_{N^{2+}} PEC^{rec})} \frac{1}{\Delta L n_{e,NII}^2}, \tag{1}$$

where ϵ_{NII} is the N II emissivity in $[W/m^3/steradian]$, ΔL is the length of the N II emitting region through the line-of-sight (LOS), $PEC^{exc,rec}$ are excitation and recombination photon emissivity coefficients [11] in $[m^3/s]$, f_{N^z} is the fractional ion abundance of the Z charged ion, and $n_{e,NII}$ is the average electron density associated with ΔL. The f_{N^z} is calculated using a zero-transport ionisation balance.

The average electron temperature of the N II emitting region, $T_{e,NII}$, must also be calculated to interpolate the temperature and density dependent $PEC^{exc,rec}$ and f_{N^z}. Comparison of the measured N II multiplet line ratios at 399.5 nm, 402.6 nm, and 404.1 nm, shown in figure 1a and 1b, with the equivalent $PEC^{exc,rec}$ ratios can provide a unique solution of $T_{e,NII}$ and $n_{e,NII}$ [11]. However, to avoid the difficulties of measuring the weak, blended line at $\lambda = 402.6$ nm over a range of pulses, only the strongest N II lines at 399.5 nm and

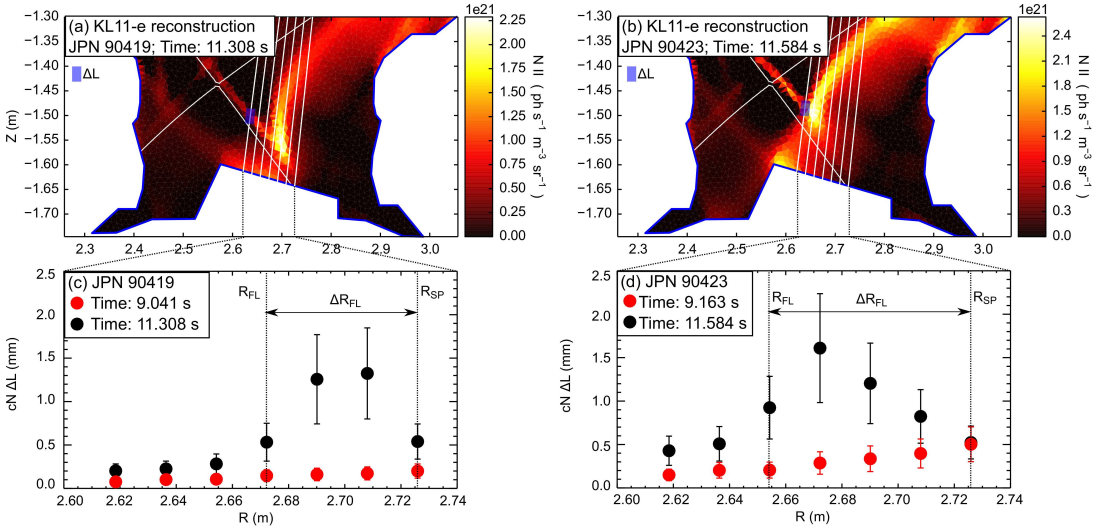

Figure 3: Inverted camera data with a narrow filter measuring the N II emission near 500 nm is shown for JET pulse numbers (a) #90419 and (b) #90423. An example of the radial $c_N \Delta L$ profile measured by spectroscopy is shown for two different times in (c) and (d).

404.1 nm are used in this work. It was shown previously that the N II emission tends to occur between $T_{e,NII} = 3.5 - 4.0$ eV [11], consistent with the assumption of zero-transport, and therefore these limits are used to interpolate the minimum and maximum $n_{e,NII}$ using the line ratio model shown in figure 1c.

3.1. Emission zones

To calculate ΔL, the line-integrated spectrometer measurements must be assessed in combination with 2D N II emission profiles in the divertor. For AUG, an inversion of the spectrometer sightlines viewing the outer divertor to obtain a rough local emissivity has been carried out for one pulse (#34971) to characterize ΔL at different T_{div}. The geometry and 2D N II emission profiles are shown in figures 2a-c for three time-windows: $t = 3 - 3.3$ s, $t = 3.5 - 4$ s, and $t = 4 - 4.5$ s corresponding to $T_{div} \approx 15$ eV, $T_{div} \approx 10$ eV, and $T_{div} \leq 5$ eV, respectively. Note the top row of (partially) unconstrained grid points which have been used to account for any additional emission emanating from the far/upstream scrape-off layer (SOL). When T_{div} is high, the fully constrained grid points are sufficient to account for the majority of emission measured by the spectrometer sightlines. However, as the temperature falls below 15 eV, the emission from the unconstrained grid points becomes more significant which is consistent with an emission front moving from the strike-point towards the X-point as divertor detachment occurs.

The ROV-11 horizontal sightline, as shown by the bold line in figures 2a-c, is used to

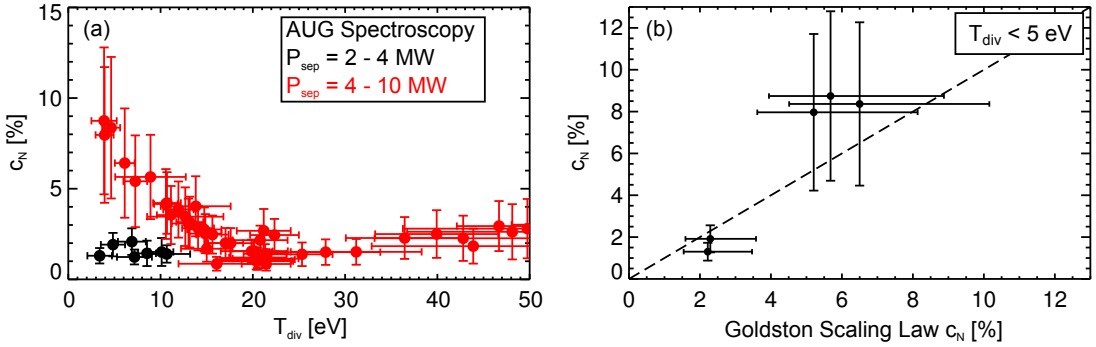

Figure 4: Spectroscopic measurements of c_N from AUG H-mode plasma are shown as a function of T_{div} in (a). The spectroscopy c_N measurements in AUG plasma with $T_{div} \leq 5$ eV are compared with scaling law predictions for detachment from Goldston *et al.* in (b).

evaluate c_N in this analysis. It is noted that the emission immediately below this sightline is unexpectedly low; however post-campaign calibrations of the sightline window transmission have been performed and included in this analysis to rule out calibration issues. Furthermore, an inversion has been carried out for a plasma with a lower strike point which consistently showed more emission in this lower region of plasma. Considering that the strike point location is not fixed in this analysis, this will yield moderately different values of ΔL to those derived from the inversion shown in figures 2a-c. This uncertainty, along with the uncertainty from the coarse grid size, is thought to lie within the two curves of ΔL for ROV-11 shown in figure 2d as a function of T_{div}. The maximum geometrical limit of this sightline is $\Delta L \approx 11$ cm.

On JET, the 2D emission profiles are determined by inverting camera images filtered for the N II emission near 500 nm, as demonstrated in figure 3a and 3b. The strong N II lines near 500 nm correspond to $3d - 3p$ and $3p - 3s$ orbital transitions which have similar temperature and density dependencies to the $3p - 3s$ N II transition line at 399.5 nm used in this analysis. Therefore, any differences in ΔL between the N II transition lines measured by the camera and the spectrometer should be negligible. Due to the vertical spectrometer line-of-sight (LOS) geometry in JET, only the sightlines which avoid significant line-integration through the detachment front region in the far SOL are considered for the c_N analysis shown in the next section because of the difficulties in estimating the ΔL through the emission front. On the other hand, the sightlines measured upstream of this front region sample only a small, localised region ($\Delta L \approx 2.5 - 3.5$ cm) near the separatrix.

To determine the radial location (along the divertor tile) of the detachment front, R_{FL}, at each time slice, the c_N measurements without the factor $1/\Delta L$ (i.e. $\Delta L c_N$ in units $[m]$) are assessed. Moving from left to right sightlines, the first $\Delta L c_N$ measurement to rise above the standard deviation is defined as R_{FL}. The radial location of the strike point, R_{SP}, is fixed at

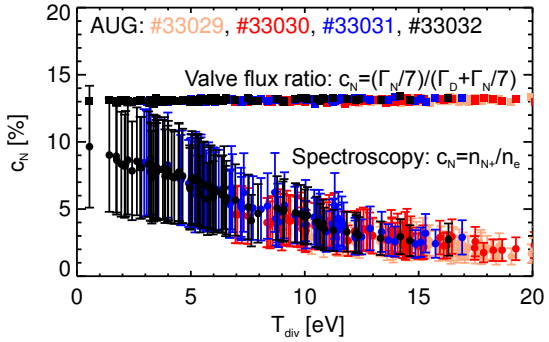

Figure 5: A comparison of the spectroscopy and gas valve flux ratio estimates of c_N are shown for four consecutive, identically setup AUG pulses.

$R_{SP} = 2.7$ m, providing a gauge of the detachment front movement ($\Delta R_{FL} = R_{FL} - R_{SP}$). An example of the $\Delta L c_N$ profile and ΔR_{FL} evaluation at a single time slice is shown in figure 3c and 3d, while the ΔR_{FL} results for both discharges are shown in full in the next section (see figure 6b).

4. Results and analysis

The spectroscopic c_N results from the H-mode AUG pulses are shown in figure 4a. Higher power measurements (red circles) show that the c_N is higher at lower T_{div}, as expected. The c_N measurements in low power plasma (black circles) are significantly lower than the equivalent c_N measurements at higher power. To further investigate the parameter dependencies of c_N in partially/detached plasma ($T_{div} \leq 5$ eV), the measurements are compared with scaling law predictions from Goldston *et al.* [7] in figure 4b. The c_N required to reach detachment can be predicted from Goldston *et al.* using

$$c_N^{scaling} = \frac{1}{18.3}\left(\frac{P_{sep}[MW]}{< B_p > [T](1+\kappa^2)^{3/2} f_{GW,sep}^2}\right) \times 4.0[\%] \tag{2}$$

where the value of 4% is from a gas valve flux ratio estimate from Kallenbach *et al.* [8] in a plasma with $P_{sep} = 10.7$ MW, $< B_p >= 0.34$, $\kappa = 1.63$, and $f_{GW,sep} = 0.496$ (thus giving the factor 18.3). From the data shown, the c_N trend in partially/fully detached plasma agrees within error bars with $c_N^{scaling}$. Note that the error for $c_N^{scaling}$ is set by allowing a factor of 1.2 and 0.8 variation on $f_{GW,sep}$.

The equivalent N concentration measurement from the gas valve flux ratio is given by

$$c_N^{flux} = \frac{\Gamma_N/7}{\Gamma_D + \Gamma_N/7} \tag{3}$$

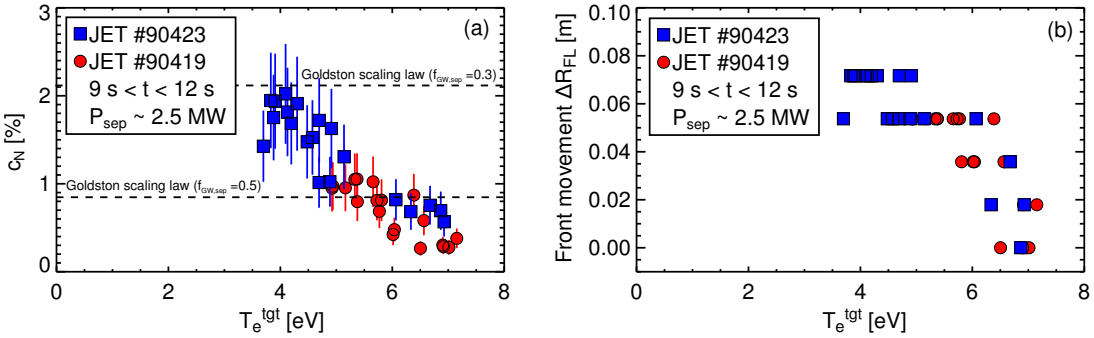

Figure 6: Spectroscopic measurements of c_N and the amount of movement of the N II emission front away from the strike point are shown as a function of the strike point temperature from Langmuir probes for two JET L-mode plasma in (a) and (b), respectively. Scaling law predictions of c_N required for detachment are indicated in (b) by the dashed lines for two values of $f_{GW,sep}$.

where Γ_Z is defined in electrons/s, and the numerator and denominator factors of seven are for counting N ions and electrons, respectively, assuming that N only contributes one electron in the divertor. A comparison of c_N and c_N^{flux} is shown in figure 5 for four consecutive, identically setup pulses on AUG which have the same, constant N_2 seeding flux (see [10]). In the first pulse, the outer divertor remains attached and the two measurements differ significantly. However, in the following pulses there is a gradual convergence of the two measurements as T_{div} falls. This convergence is thought to be strongly correlated with the vessel wall conditions. When the vessel walls are fully-loaded, and the release of N occurs at a similar rate to the pumping of N, there is agreement between c_N and c_N^{flux} within the error bars of c_N. These particular series of pulses were carried out with moderate $P_{sep} \approx 5$ MW which could explain the relatively long time (4 pulses) to reach agreement. At higher power, the two measurements may reach agreement in a shorter timescale; additionally, the timing of the pulse relative to the last boronisation could also affect the measurement.

Lastly, the spectroscopic c_N measurements from the two L-mode JET pulses are shown in figure 6a as a function of T_e^{tgt} (recall now the use of the Langmuir probe temperature, T_e^{tgt}, rather than T_{div}). Like AUG, the c_N is higher for lower T_e^{tgt}. The dashed lines indicate the $c_N^{scaling}$ calculated at two estimates of $f_{GW,sep} = 0.3$ and $f_{GW,sep} = 0.5$. It is noted that the $c_N^{scaling}$ prediction for L-mode plasma will likely be lower than the results shown due to the larger scrape-off layer width compared to H-mode. Figure 6b shows the ΔR_{SP} as a function of T_e^{tgt} to demonstrate the algorithm for detecting R_{FL}. This shows a clear movement of the front away from the strike point as divertor plasma cools.

5. Conclusions

This first assessment of spectroscopic N concentration measurements in both AUG and JET divertor plasma demonstrates the application of a new measurement technique over a wide range of plasma conditions. For plasma with similar power crossing the separatrix, the measurements show that higher N concentrations lead to lower divertor temperatures, as expected given the higher power losses. Furthermore, for plasma with partially or fully detached outer divertor plasma, the N concentration required to reach the same target temperature increases with the power crossing the separatrix. Recovering these expected trends builds confidence in the measurement technique and lays the foundations for further parameter dependency studies.

The uncertainties of the spectroscopic measurement are mainly driven by the temperature and density predictions of the emission region, since the intensity of emission varies logarithmically with temperature while the concentration varies inversely to the density squared. Including additional N II spectral lines to constrain the predictions could reduce the uncertainty, however these predictions would be more robust combined with other measurements of the temperature and density, for example a divertor Thomson scattering diagnostic. The effect of plasma transport, electron excitation driven by molecular dissociation, the length of the emitting region, and the atomic structure accuracy also play a role in defining the total uncertainty, however these contribute less significantly in comparison to the temperature and density predictions.

In general, the absolute magnitudes of the N concentrations from spectroscopy agree with estimates derived from the N and D gas valve flux rates if there has been significant N_2 seeding beforehand and the vessel surfaces are fully-loaded. Scenarios with a low background N concentration before seeding can result in deviations of up to an order magnitude between the two measurements. These initial results therefore suggest that the vessel wall conditions, specifically the amount of N released from the wall, must be considered if using gas valve flux rates in a 'feed-forward' (non-feedback) mode to control the divertor state with respect to detachment. A benefit of the spectroscopic measurement, in addition to the fact that it is spatially resolved in (at-least) 1D, is that the vessel wall conditions do not appear to affect the measurement.

Lastly, spectroscopic measurements of the N concentration from different devices with relatively similar scrape-off layer plasma conditions could provide an insight into the complicated divertor geometry effects which can significantly impact the plasma conditions required for detachment. However, examination of specific parameter dependencies and trends within a single device and configuration, such as the separatrix power and poloidal magnetic field, may offer a more reliable understanding for optimizing future configurations.

Acknowledgements

This work has been carried out within the framework of the EUROfusion Consortium and has received funding from the Euratom research and training programme 2014-2018 under grant agreement No 633053 and from the RCUK Energy Programme [grant number EP/P012450/1]. To obtain further information on the data and models underlying this paper please contact PublicationsManager@ukaea.uk. The views and opinions expressed herein do not necessarily reflect those of the European Commission.

References

[1] E. A. Lazarus *et al.*, Nucl. Fusion **25**, 135 (1985).

[2] A. Kallenbach *et al.*, Nucl. Fusion **35**, 1231 (1995).

[3] J. Rapp *et al.*, Nucl. Fusion **44**, 312 (2004).

[4] J. A. Goetz *et al.*, Phys. Plasmas **6**, 1899 (1999).

[5] J. A. Goetz *et al.*, J. Nucl. Mater. **266**, 354 (1999).

[6] M. Groth *et al.*, Nucl. Fusion **42**, 591 (2002).

[7] R. J. Goldston, M. L. Reinke, and J. A. Schwartz, Plasma Phys. Control. Fusion **59**, 055015 (2017).

[8] A. Kallenbach *et al.*, Plasma Phys. Control. Fusion **58**, 045013 (2016).

[9] A. Kallenbach *et al.*, this conference, to be published in Nuclear Materials and Energy (2018).

[10] A. Drenik *et al.*, this conference, to be published in Nuclear Materials and Energy (2018).

[11] S. S. Henderson *et al.*, Nucl. Fusion **58**, 016047 (2018).

[12] S. Potzel *et al.*, Plasma Phys. Control. Fusion **56**, 025010 (2014).

[13] B. A. Lomanowski *et al.*, Nucl. Fusion **55**, 123028 (2015).

[14] A. Kallenbach *et al.*, Nucl. Fusion **55**, 053026 (2015).

[15] A. Meigs *et al.*, Rev. Sci. Instrum. **81**, 10E532 (2010).

[16] B. A. Lomanowski *et al.*, this conference, to be published in Nuclear Materials and Energy (2018).